16.9   A 20Gb/s 79.5mW 127GHz CMOS Transceiver with Digitally Pre-Distorted PAM-4 Modulation for Contactless Communications

Yanghyo Kim[1,2], Boyu Hu[2], Yuan Du[2], Adrian Tang[1,2], Huan-Neng Chen[3], Chewnpu Jou[3], Jason Cong[2], Tatsuo Itoh[2], Mau-Chung Frank Chang[2,4]

[1]Jet Propulsion Laboratory, Pasadena, CA
[2]University of California, Los Angeles, CA
[3]TSMC, Hsinchu, Taiwan
[4]National Chiao Tung University, Hsinchu, Taiwan

Contactless chip-to-chip or board-to-board proximity (~1mm) communications have been realized by using either wireless transmission [1-3], or inductive/capacitive coupling schemes [4-6]. However, their practical deployments in consumer electronics are currently limited because of bandwidth-density-inefficient OOK/ASK-only modulations [1-3], process/voltage/temperature sensitive carrier-recovery-less coherent detection [1], and large coupler footprint (6~10mm²) for meeting bandwidth requirements [1], [4-6]. To overcome such challenges, the demonstrated contactless communication system employs a 127GHz CMOS transceiver to concurrently increase the coupling bandwidth and reduce coupling antenna size. Furthermore, a PAM-4 modulator with digital pre-distortion (DPD) in the transmitter (TX) and an envelope detecting non-coherent receiver (RX) are designed to further scale the bandwidth and eliminate carrier recovery circuitry, respectively.

The block diagram of the CMOS transceiver with a 127GHz carrier and digitally pre-distorted PAM-4 modulation is shown in Fig. 16.9.1. Unlike a conventional wireless TX that demands a linear mixer and power amplifier, the implemented TX uses only an oscillator to deliver the necessary output power and mixes signals via a capacitive-digital-to-analog-converter (CDAC) based rail-to-rail PAM-4 modulator. The PAM-4 modulator consists of three 5b CDACs, each of which is responsible for the height of one distinct data-eye. The RX contains a one-stage low-noise amplifier (LNA), a down-conversion self-mixer, and extra output drivers to interface with an oscilloscope for testing purposes. As illustrated in Fig. 16.9.1, the TX mixer encounters non-linearity through a rail-to-rail PAM-4 input swing, and the RX self-mixer also conducts a non-linear square-law operation. Consequently, equally spaced PAM-4 input signals end up with unequal spacing at the RX output. Thus, to invert the system non-linearity, three parallel 5b CDACs pre-distort the input signals through symbol re-mapping in a memoryless way.

As simulated in Fig. 16.9.1, an efficient air-coupling between TX and RX is achieved by designing a folded-dipole antenna on FR4HR substrate similar to that of [3]. To retain sufficient bandwidth while maintaining a differential input impedance of 100Ω, asymmetrical thicknesses of the upper (0.076mm) and lower (0.103mm) conductor are chosen. A via-wall (3 mil spacing between each via) is also placed around the antenna to confine electromagnetic energy in case of implementing multi-channel systems. The resulting footprint of the antenna is 0.7mm², and the radiation pattern of E- and H-plane shows 5.9dBi gain. According to HFSS simulations, 1mm air-coupling causes 7dB loss at 127GHz, and 1mm offset in x- and y-axis contributes 10dB extra loss.

The CDAC-based PAM-4 modulator of TX is shown in Fig. 16.9.2. A cascade of a 32:4 MUX and a 4:2 MUX up-streams baseband parallel signals to the full symbol rate. Next, a 2:3 decoder splits the 2b PAM-4 data stream into a 3b thermo-code signal D[2:0] with each bit mapping to one of the three PAM-4 eyes. The CDAC is composed of three identical sub-sections, each of which contains binary-weighted 5b capacitors and their driver/data-select-MUX. Through a 3:1 MUX, each weighted capacitor can be assigned to any of the 3b thermo-codes. In such a way, the weight percentage of an individual data-eye over the total amount can be independently adjusted while keeping the PAM-4 modulator swing constant. As an example, when the 'sel1_16[2:0]' of 'DPD code 1' is set [100] instead of [010], an extra 16C portion is assigned to the upper-eye CDAC by borrowing from the center-eye CDAC, to widen the upper-eye and shrink the center-eye, while leaving the lower-eye unchanged. In addition, the PAM-4 modulator adjusts its output common-mode (CM) via an R-2R DAC to optimize the biasing point of the mixer. This allows the PAM-4 waveform at the mixer input to be digitally pre-distorted within the rail-to-rail range.

In the TX circuitry depicted in Fig. 16.9.3, a free-running oscillator generates 127GHz carrier and drives the switching pair of a single-balanced mixer via a transformer. The mixer's input/output characteristic can be comprehended by sweeping the DC bias of the tail device and measuring the peak-to-peak swing of the 127GHz carrier at the TX output. As shown in the simulated plot, the gain of the mixer is higher when the input is in between upper and lower rail. Correspondingly, the center-eye is expected to grow wider than the rest. Comparing simulated waveforms with and without DPD, the carrier's modulation depth becomes more evenly spaced at the TX output by reducing center-eye amplitude at the mixer input. Note that the carrier's modulation depth at the TX output gradually decreases from the digital state 00 to 11. This is to compensate for the square-law non-linearity of the self-mixer in the RX, where gain increases from lower to larger input swings. Finally, the TX delivers -0.2dBm saturated output power under 1.2V supply.

In the RX path shown in Fig. 16.9.4, an LNA amplifies incoming signals with 10dB gain while offering 9dB noise figure (NF). After integrating over 10GHz (100dB) LNA bandwidth, the RX sets the noise floor at -65dBm [-174dBm/Hz + 100dB + 9dB]. Assuming the 17dB worst-case air-coupling loss from Fig. 16.9.1, the self-mixer receives a -7.2dBm [-0.2 dBm (TX) - 17dB + 10dB (LNA)] carrier-modulated signal and yields 20dB conversion loss based on its simulated input/output characteristic. To increase the demodulation bandwidth of the self-mixer, a feedback trans-impedance amplifier is designed as a load to convert the rectified current into voltage. With a -27.2dBm [-7.2dBm-20dB] de-modulated signal and considering 27dB to be the minimum signal-to-noise ratio (SNR) required to achieve a bit-error-rate (BER) better than 10^{-12} for intended PAM-4 signaling, the system exhibits an SNR margin of 10.8dB [-27.2dBm - (-65dBm + 27dB)]. At the output of the self-mixer, an RC filter extracts the average DC content of the demodulated signal. Because of the data-pattern-dependent average DC level of PAM-4 signaling, an R-2R DAC feeds a constant CM to the single-ended-to-differential converter (SDC) based on feedback from the RC filter. Additionally, to prevent a mismatch-oriented DC offset from propagating through the SDC and following output drivers, an offset cancellation is embedded in the SDC using R-2R DACs and digitally controlled current sources. Comparing simulated waveforms, de-modulated PAM-4 signals display four balanced levels with DPD whereas PAM-4 signals without DPD produce three unequal levels instead.

The prototype TX and RX are implemented in a 65nm CMOS process and are tested by placing them 1mm apart from each other as shown in Fig. 16.9.7. As captured in Fig. 16.9.5, without DPD, upper-eye is completely closed, center-eye is widely opened, and lower-eye is almost closed. Once DPD is applied, all three levels open equally, fulfilling 20Gb/s data communication. The amplitude of each eye opening shown by the oscilloscope is relatively small (~10 mV), because the RX output driver transports the de-modulated PAM-4 signal linearly. The BER is estimated to be superior to 10^{-12} according to measured eye openings and calculated SNR. The fabricated TX and RX are shown in Fig. 16.9.7. The entire contactless communication system consumes 79.5mW (TX: 50.8mW, RX: 28.7mW) without counting input/output drivers, resulting in 3.98pJ/b energy efficiency. Figure 16.9.6 summarizes and compares its performance with that of prior arts. This work accomplishes a 127GHz CMOS transceiver with digitally pre-distorted PAM-4 modulation for reaching state-of-the-art data rate and energy efficiency.

References:
[1] Y. Tanaka, et al., "A versatile multi-modality serial link," *ISSCC*, pp. 332-333, Feb. 2012.
[2] Y. Kim, et al., "A 60 GHz CMOS transceiver with on-chip antenna and periodic near field directors for multi-Gb/s contactless connector," *IEEE Microwave Wireless Component Letters*, vol. 27, no. 4, pp. 404-406, Mar. 2017.
[3] Y. Kim, et al., "A 125 GHz transceiver in 65 nm CMOS assembled with FR4 PCB antenna for contactless wave-connectors," *IEEE MTTS Int. Microwave Symp.*, June 2017.
[4] A. Kosuge, et al., "A 6 Gb/s 6 pJ/b 5 mm-distance non-contact interface for modular smartphones using two-fold transmission-line coupler and EMC-qualified pulse transceiver," *ISSCC*, pp. 176-177, Feb. 2015.
[5] K. Hijioka, et al., "A 5.5 Gb/s 5mm contactless interface containing a 50 Mb/s bidirectional sub-channel employing common-mode OOK signaling," *ISSCC*, pp. 406-407, Feb. 2013.
[6] C. Thakkar, et al., "A 32 Gb/s bidirectional 4-Channel 4 pJ/b capacitively coupled link in 14 nm CMOS for proximity communication," *IEEE JSSC*, vol. 51, no. 12, pp. 3231-3245, Dec. 2016.
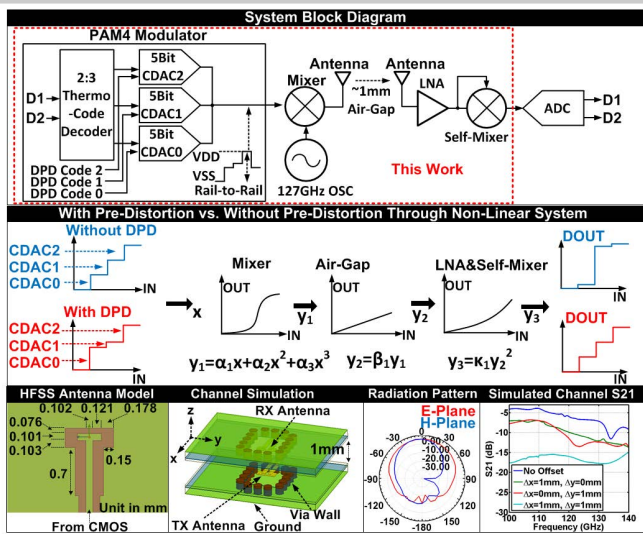
Figure 16.9.1: System block diagram, digital pre-distortion concept, and air-coupling design.
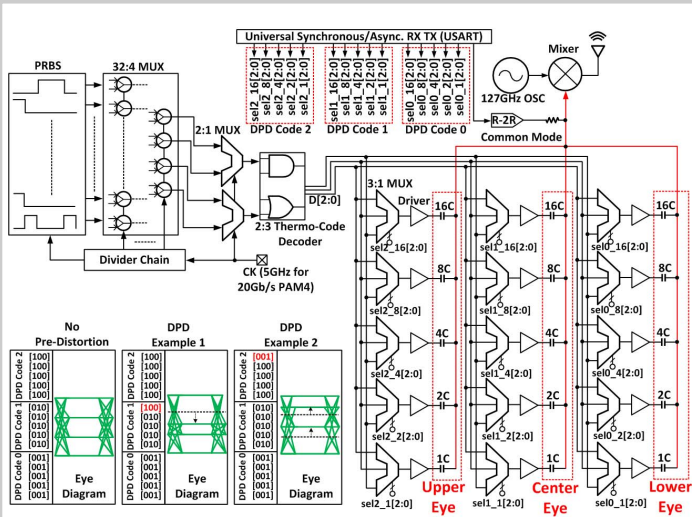

Figure 16.9.2: Schematic of capacitive-DAC-based PAM-4 modulator with memoryless DPD examples.
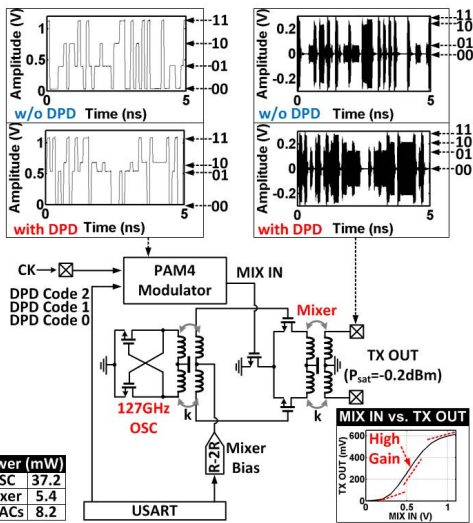

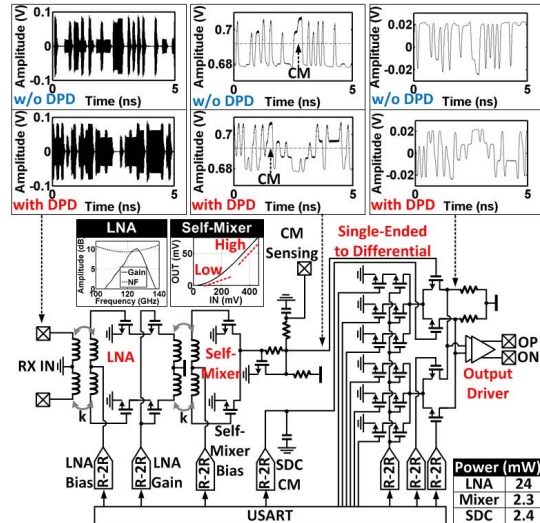Figure 16.9.3: Schematic of CMOS TX, and simulated waveforms with and without DPD.

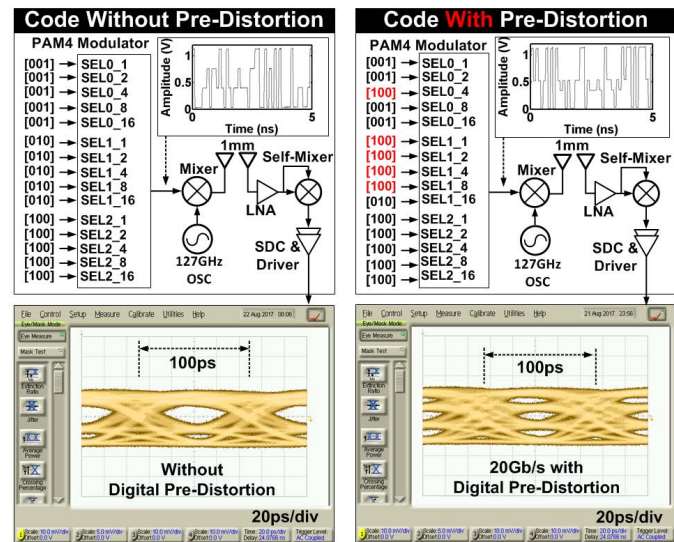Figure 16.9.4: Schematic of CMOS RX, and simulated waveforms with and without DPD.

Figure 16.9.5: Measured eye-diagrams with and without DPD.

	This Work	ISSCC 2012 [1]	MWCL 2017 [2]	IMS 2017 [3]	ISSCC 2015 [4]	ISSCC 2013 [5]	JSSC 2016 [6]
Coupling Method	Antenna	Antenna	Antenna	Antenna	T-Line	Inductive	Capacitive
Carrier (GHz)	127	57 & 80	60	125	Baseband	Baseband	Baseband
Modulation	PAM4 (Non-Coherent)	ASK (Coherent)	OOK (Non-Coherent)	OOK (Non-Coherent)	N/A	N/A	N/A
Technology	65nm CMOS	40nm CMOS	65nm CMOS	65nm CMOS	65nm CMOS	0.18μm CMOS	14nm CMOS
Data Rate (Gb/s)	20	20	5	14	6	5.5	8
Power (mW)	79.5	137	40	60	36	198	32
FoM (pJ/bit)	3.98	6.85	8	4.3	6	36	4
Coupler Footprint (mm²)	0.7	9	0.2	0.9	1.11	N/A	9.6
Distance (mm)	1	5	0.5	2	1.11	5	0.8

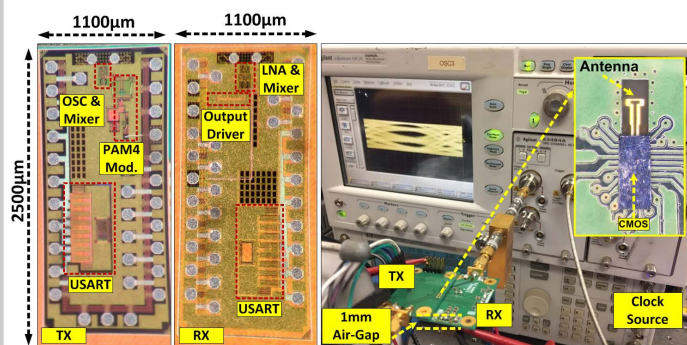Figure 16.9.6: Performance comparison table.

16

Figure 16.9.7: TX and RX die photo, measurement setup, and flip-chip assembled module.